



ELSEVIER

J. Non-Newtonian Fluid Mech. 81 (1999) 215–234

**Journal of
Non-Newtonian
Fluid
Mechanics**

Instability due to second normal stress jump in two-layer shear flow of the Giesekus fluid

Yuriko Y. Renardy*, Michael Renardy

Department of Mathematics and ICAM, Virginia Polytechnic Institute and State University, Blacksburg, VA 24061-0123, USA

Received 14 January 1998; received in revised form 26 May 1998

Abstract

The two-layer Couette flow of superposed Giesekus liquids is examined. In order to emphasize the effect of a jump in the second normal stress difference, the analysis is focused on flows where the shear rate and first normal stress difference are continuous across the interface. In this case, the flow is neutrally stable to streamwise disturbances, but can be unstable for spanwise disturbances driven by a jump in the second normal stress difference. Whether the long and order one waves are stable or not depends on the sign of this difference. Short waves are unstable. In the case of order one wave instability, the mode of maximum growth rate gives rise to stationary ripples perpendicular to the flow. The eigenvalue problem for purely spanwise wave vectors can in principle be solved analytically, although, in general, the analytical solution is too complicated to obtain. In most cases, however, a simplifying assumption can be made which makes analytical solutions feasible. We present such solutions and compare them with purely numerical solutions. © 1999 Elsevier Science B.V. All rights reserved.

1. Introduction

It is well known for a variety of constitutive models that a jump in the first normal stress difference N_1 across an interface drives an interfacial instability. This was demonstrated for two-layer Couette flow of upper-convected Maxwell liquids for short waves in [9] and for long waves in [1]; the problem has since been analyzed further in numerous other publications [2,5–7,10–14]. In two-dimensional channel flows of viscoelastic liquids, this mechanism can lead to 2D instabilities and has been examined, for instance, for Poiseuille flow of Oldroyd-B fluids [14]. The role of the first and second normal stress differences on interfacial instability is further discussed in [1,2,5]. In [5], a model problem consisting of Newtonian Stokes flow driven by viscoelastic stress contributions at the interface is examined to show qualitative features of an interfacial instability. A jump in the second normal stress difference across the interface can lead to 3D instabilities. In this paper, we focus on purely 3D instabilities driven by a jump in the second normal stress difference across the interface.

* Corresponding author. Fax: +1-540-231-5960.

To simplify the analysis, we investigate the stability of two-layer Couette flow of immiscible Giesekus liquids, with equal densities, zero interfacial tension, matched shear rates and matched shear-rate dependent viscosities across the interface. This eliminates the effects of density stratification, viscosity stratification, and by also matching the first normal stress differences, we eliminate that class of mechanisms for interfacial instability. Thus instability at the interface is determined purely by the jump in the second normal stress difference. The dominant mode of instability in this case is shown to consist of spanwise corrugations to the interface. For the spanwise modes which we consider, we find that short waves are always unstable, with a growth rate approaching a constant as the wave number approaches infinity. For long waves, on the other hand, stability or instability depends on the depth ratio; we find that long waves are stable if the fluid with the smaller second normal stress difference occupies the thinner region and unstable in the opposite case. If there is a first normal stress difference as well as a second normal stress difference across the interface, then we expect instabilities for both streamwise and spanwise wave number, with a possibility of maximum growth occurring for oblique waves. We present results confirming that this is the case, in agreement with recent work by Khomami and his collaborators (private communication). Three-dimensional instabilities were observed in experiments [15], and second normal stress jumps may be a contributing factor.

In principle, the linear eigenvalue problem for spanwise disturbances can be solved analytically in closed form. In general, however, this problem turns out to be so complex that it is intractable, even with symbolic manipulation packages. A considerable simplification occurs, however, if it is assumed that the characteristic time for the growth of the instability is long relative to the viscoelastic relaxation time; this is the case in all our examples. If this assumption is made, the problem is still too complicated to produce a “formula” for the growth rate, but it is possible to compute it using an algorithm based purely on symbolic manipulation and involving no numerical discretization. We present the results of such calculations and compare with the numerical results.

If the assumption of slow growth of the interfacial mode is dropped, a much more complicated problem arises. In the short wave limit, one may assume an eigenmode which decays exponentially away from the interface and does not feel the effect of boundaries [9]. There is, however, more than one such mode; recall that the analysis of two-layer Couette flow of the upper convected Maxwell fluid reveals five such modes. In the present situation, the growth rate for short wave modes is determined by a polynomial equation, but the polynomial is of very large degree, and calculating it is beyond current capabilities in symbolic manipulation. We therefore ask the mathematically similar, but tractable, question of whether there are eigenmodes in a single-fluid flow which decay exponentially away from the wall (“wall modes”). Recall that for streamwise perturbations in Couette flow of the upper convected Maxwell fluid [3], such modes are known as the Gorodtsov–Leonov modes. For spanwise perturbations in the Giesekus model, however, we show the non-existence of wall modes.

2. Governing equations

The flow geometry is shown in Fig. 1. Fluid 2 lies over fluid 1. Densities are equal and are denoted ρ , zero shear rate viscosities μ_i , and relaxation times λ_i for fluid i . The walls are located at $z^* = 0, l^*$. Asterisks are used for dimensional variables. In the basic flow, fluid 1 occupies $0 \leq z^* \leq l_1^*$ and fluid 2

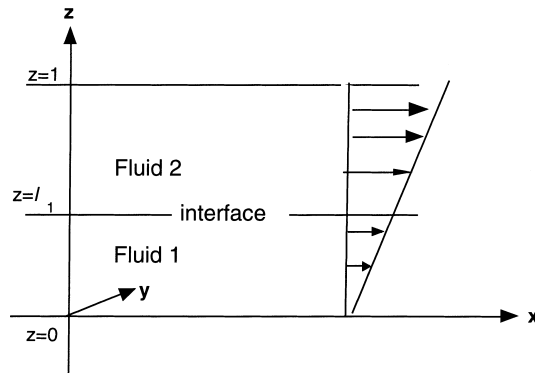


Fig. 1. Flow schematics.

occupies $l_1^* \leq z^* \leq l^*$. The velocity of the upper plate in the basic flow is denoted $(U_p, 0, 0)$. The velocity, distance, time and pressure are made dimensionless with respect to U_p , l^* , l^*/U_p , and $\mu_1 U_p / l^*$. The extra stress components are scaled the same as the pressure. The bottom plate is at rest. A Reynolds number is defined based on the parameters of fluid 1: $R_1 = \rho U_p l^* / \mu_1$. Weissenberg numbers are denoted by $W_1 = U_p \lambda_1 / l^*$ and $W_2 = U_p \lambda_2 / l^*$.

The dimensionless equation of motion is

$$R \left[\frac{\partial \mathbf{u}}{\partial t} + \mathbf{u} \cdot \nabla \mathbf{u} \right] = \nabla \cdot \mathbf{T} - \nabla p, \tag{1}$$

where \mathbf{T} is the extra stress tensor.

The Giesekus model has the constitutive relation

$$W_i \left[\frac{\partial \mathbf{T}}{\partial t} + (\mathbf{u} \cdot \nabla) \mathbf{T} - (\nabla \mathbf{u}) \mathbf{T} - \mathbf{T} (\nabla \mathbf{u})^T + \kappa_i \mathbf{T}^2 \right] + \mathbf{T} = \left[\frac{\mu_i}{\mu_1} \right] (\nabla \mathbf{u} + (\nabla \mathbf{u})^T). \tag{2}$$

At the interface, the velocity and tractions are continuous, and the kinematic free surface condition holds.

The dimensionless parameters characterizing the problem are l_1 , W_1 , W_2 , κ_1, κ_2 , R_1 and $m = \mu_1 / \mu_2$.

The dimensionless basic velocity for parallel shear flow has the form $(U(z), 0, 0)$ in the unperturbed fluid 1 ($0 \leq z \leq l_1$), and fluid 2 ($l_1 \leq z \leq 1$). In each fluid, the basic extra stress tensor has the form

$$\mathbf{T} = \begin{pmatrix} C_1 & 0 & C_2 \\ 0 & 0 & 0 \\ C_2 & 0 & C_3 \end{pmatrix}. \tag{3}$$

The base flow normal stress balance is $[[P]] = [[C_3]]$ at $z=l_1$. The basic shear stress condition is $[[C_2]] = 0$ at $z=l_1$.

Solutions that are perturbations of the basic flow are sought. The perturbations to the velocity, pressure and interface position are denoted by (u, v, w) , p and h , respectively. The perturbation to the

extra stress tensor is

$$\begin{pmatrix} T_{11} & T_{12} & T_{13} \\ T_{12} & T_{22} & T_{23} \\ T_{31} & T_{32} & T_{33} \end{pmatrix}. \tag{4}$$

The perturbation equations are given in the appendix.

2.1. Couette flow

We now focus on the case where the shear rate is continuous across the interface, so that $U(z)=z$ and $U'=1$ in both fluids. The stress components are constants in each fluid and satisfy

$$W_i[\kappa_i(C_1^2 + C_2^2) - 2C_2U'] + C_1 = 0, \tag{5}$$

$$W_i[\kappa_i C_2(C_1 + C_3) - C_3U'] + C_2 = \frac{\mu_i U'}{\mu_1}, \tag{6}$$

$$W_i \kappa_i (C_2^2 + C_3^2) + C_3 = 0. \tag{7}$$

These simplify to a single equation for C_2

$$\begin{aligned} & -C_2U'A + C_2^2\kappa_iA + U'^2A^2 + C_2U'\kappa_iA^2 - C_2^2\kappa_i^2A^2 - 2U'^2\kappa_iA^3 + U'^2\kappa_i^2A^4 - C_2^3U'\kappa_iW_i^2 \\ & + C_2^4\kappa_i^2W_i^2 - 2C_2^2U'^2\kappa_iAW_i^2 + 8C_2^3U'\kappa_i^2AW_i^2 - 4C_2^4\kappa_i^3AW_i^2 + 2C_2^2U'^2\kappa_i^2A^2W_i^2 \\ & - 8C_2^3U'\kappa_i^3A^2W_i^2 + 4C_2^4\kappa_i^4A^2W_i^2 + C_2^4U'^2\kappa_i^2W_i^4 = 0, \quad A = \frac{\mu_i}{\mu_1}. \end{aligned} \tag{8}$$

For given fluid parameters and shear rate, Eq. (8) yields C_2 as a solution of a quartic equation. For $A\kappa_i < 1$, this quartic equation has two complex roots and two real roots. Figs. 2 and 3 show the two possible behaviors in the two real roots of Eq. (8) as a function of the shear rate U' . The physically relevant solution is the one which approaches the origin with slope A ; the other solution has the wrong slope, and it can also be shown to produce non-zero normal stress differences at zero shear rate. This second solution is an artifact of the Giesekus model with no physical relevance. The figures show typical behavior for the two cases $A\kappa_i < 0.5$ (Fig. 2) and > 0.5 (Fig. 3). We choose to work in the range

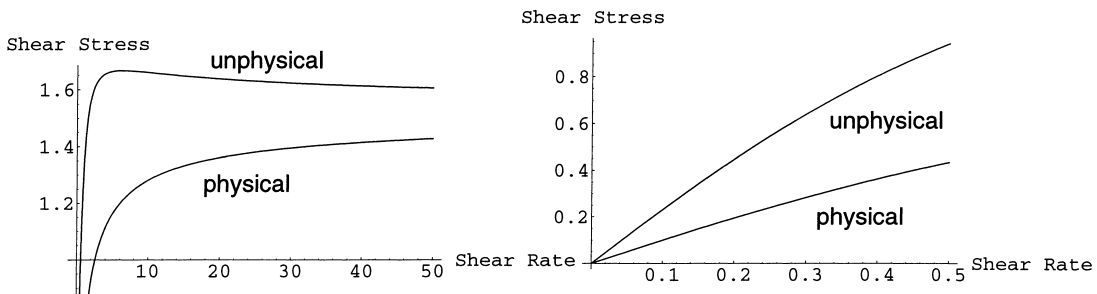


Fig. 2. Shear stress C_2 of the base flow vs shear rate U' for $A=1$, $W_i=1$, $\kappa_i=0.3$ showing the physical and unphysical branches for (a) large shear rates and (b) small shear rates.

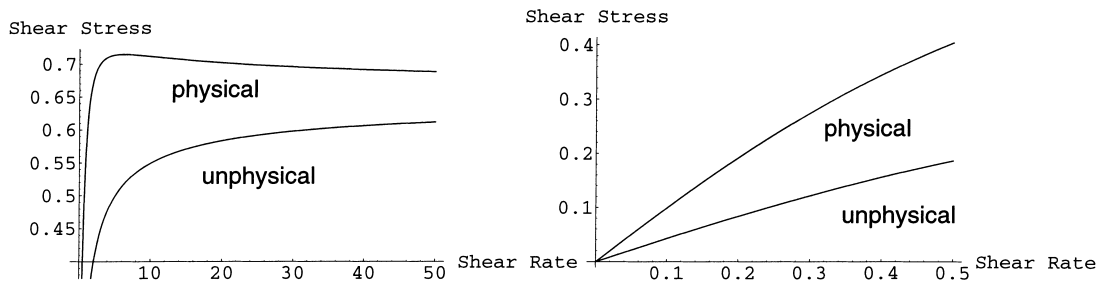


Fig. 3. Shear stress C_2 of the base flow vs shear rate U' for $A=1, W_i=1, \kappa_i=0.7$ showing the physical and unphysical branches for (a) large shear rates and (b) small shear rates.

$A\kappa_i < 1/2$, where the physically relevant solution is the smaller one, which does not go through a shear stress maximum [4]. If $A\kappa_i > 1/2$, the physically relevant solution is the larger one, and the shear stress attains a maximum at a certain shear rate. Once C_2 is known, Eq. (5) and Eq. (7) yield C_1 and C_3 as solutions of quadratic equations. The Eq. (5) has a positive and a negative root for C_1 . The positive root tends to zero as U' and C_2 approach zero, and it is the physically relevant one, while the negative roots approaches $-1/(W_i\kappa_i)$. The Eq. (7) has two negative roots for C_3 ; the physically relevant one is the one which is smaller in modulus and tends to zero at zero shear rate.

3. Matching the N_1 , shear rates and local viscosities

In contrast to a jump in the first normal stress difference across the interface which is known to drive a 2D interfacial instability, we focus on the three-dimensional instability driven by a jump in the second normal stress difference across the interface. This is done by making the base field continuous in the shear rate U' , shear stress C_2 , and first normal stress difference $N_1=C_1-C_3$, while keeping a jump across the interface in the second normal stress difference $N_2=C_3$. We also set equal density and zero interfacial tension.

The following algorithm yields the desired result. First, set the parameters for fluid 1; i.e. choose l_1, κ_1, R_1, W_1 . We prescribe the velocity gradient $U'=1$ for both fluids, and the calculation of Section 2.1 yields the stresses in fluid 1. We next determine the conditions of fluid 2. The shear stress C_2 and first normal stress difference N_1 for fluid 2 are those of fluid 1. There are then four unknowns in fluid 2: W_2, κ_2 , the viscosity ratio $m=\mu_1/\mu_2$, and C_3 . The constitutive equations yield 3 equations, so that during the solution process, a parameter (q below) can be prescribed arbitrarily. Subtract Eq. (5) from Eq. (7):

$$C_1 - C_3 + (C_1 - C_3)(C_1 + C_3)\kappa_2 W_2 - 2C_2 W_2 = 0. \tag{9}$$

We replace C_1-C_3 by N_1 , and divide the resulting equation by N_1 to obtain

$$1 + (C_1 + C_3)\kappa_2 W_2 = 2C_2 W_2 / N_1. \tag{10}$$

This is substituted into the coefficient of C_2 in Eq. (6):

$$-1/m - C_3 W_2 + 2C_2^2 W_2 / N_1 = 0,$$

Table 1

Fluid 1 parameters are $l_1=0.3$, $R_1=0.001$, $\kappa_1=0.4$, $W_1=5/3$, $C_1=0.902$, $C_2=0.479$, $C_3=-0.173$. Fluid 2 parameters are tabulated for selected values of $q=\kappa_2/m$

W_2	C_1	C_3	q	m	κ_2
1.6087	0.942	-0.132	0.3	1.111	0.3333
1.62215	0.935	-0.140	0.318	1.0877	0.3459
1.6848	0.8685	-0.206	0.48	0.9373	0.4499

which yields

$$C_3 = 2C_2^2/N_1 - 1/(mW_2). \quad (11)$$

This is substituted in $C_1=N_1+C_3$, which is substituted in Eq. (10):

$$1 - 2C_2W_2/N_1 + \kappa_2W_2(4C_2^2/N_1 + N_1 - 2/(mW_2)) = 0. \quad (12)$$

The expression for C_3 is substituted into Eq. (7):

$$2C_2^2/N_1 - 1/(mW_2) + \kappa_2W_2(C_2^2 + 4C_2^4/N_1^2 + 1/(m^2W_2^2) - 4C_2^2/(mN_1W_2)) = 0. \quad (13)$$

We prescribe $q=\kappa_2/m$ since we have one free parameter. We want fluid 2 to be also one which has a monotone shear-stress/shear-rate curve, and for this we require that $\kappa_2/m < 0.5$. We set $\kappa_2=qm$ in Eq. (13), to obtain a quadratic equation for mW_2 :

$$q - 1 + mW_2(2C_2^2/N_1 - 4C_2^2q/N_1) + (mW_2)^2(C_2^2q + 4C_2^4q/N_1^2) = 0. \quad (14)$$

This yields two possible values for mW_2 , one of which is unphysical. In Eq. (12), replace κ_2 by qm and obtain an equation that contains both m and mW_2 , and use the calculated value for mW_2 to find m .

In Table 1, we show a sample case at low Reynolds number $R_1=0.001$ and $\kappa_1=0.4$. The interface position is $l_1=0.3$. We set $W_1=5/3$. These yield the stress values given in the table.

The effect of varying q over the range 0 to 0.5 (the physically relevant range described in Section 2.1) is shown in Fig. 4. The parameters for fluid 1 are those of Table 1: $l_1=0.3$, $R_1=0.001$, $\kappa_1=0.4$, $W_1=5/3$, $C_1=0.902$, $C_2=0.479$, $C_3=-0.173$.

4. Numerical results on 3D modes

For the linear stability analysis, we discard terms that are quadratic or higher in the perturbations and seek normal mode solutions u, v, w, p, T_{ij} and h which are proportional to $\exp(i\alpha x + i\beta y + \sigma t)$, where σ denotes complex-valued eigenvalues which are solved with the other parameters given. The details of the discretization, such as the Chebyshev-tau scheme [8], are given in [11] and are not repeated here. The linear code has been checked with an independent code that takes the eigenpair and reconstructs the governing equations.

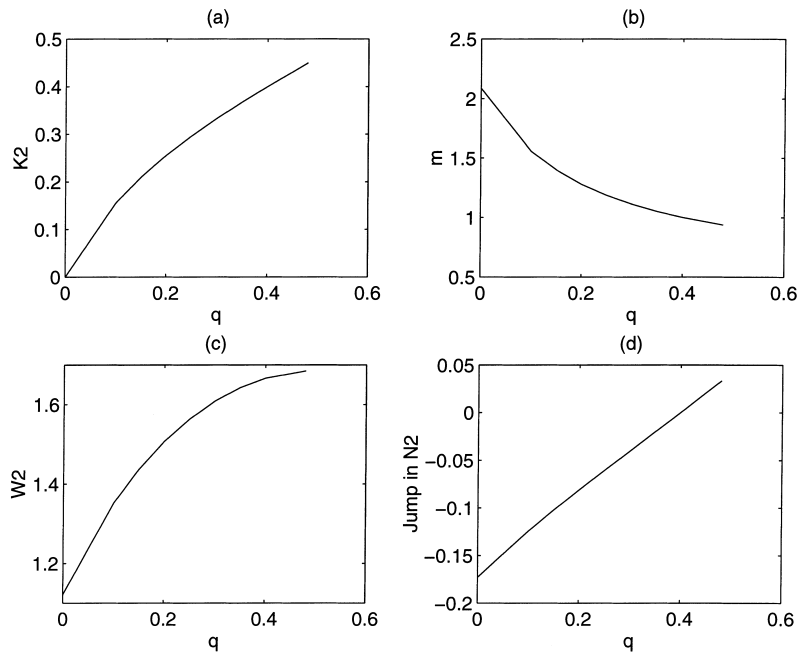


Fig. 4. The variation with q of the base flow variables (a) κ_2 , (b) m , (c) W_2 , (d) $[[N_2]] = C_3$ (of fluid 1) $- C_3$ (of fluid 2) for the conditions of Table 1.

4.1. Maximum growth rate modes

The growth rates vs wavenumbers for the first data set in Table 1 is shown in Fig. 5. The maximum growth rate is attained at $\alpha=0$, $\beta \approx 3.5$. This means that although oblique traveling waves can be excited, the dominant mode is the one perpendicular to the flow direction. At $\alpha=0$, the interfacial eigenvalues are real-valued, hence this instability would be observed as spanwise corrugations (standing waves) in the flowfield. Fig. 6 shows the growth rates for two different values of α . Evidently, as β increases in both cases, the growth rates approach the same constant value.

4.2. Spanwise modes

We next focus on the case $\alpha=0$ for which the maximum growth or decay rate is achieved. The growth rate for long waves, β small, is proportional to $[[N_2]]$. This is illustrated in Fig. 7(b), which shows that growth rates for $[[N_2]] = \pm 0.0332$ are mirror images. Fig. 7(a) shows that the growth rates are approximately mirror images over a wide range of β , but that for $\beta \rightarrow \infty$, the asymptotic behavior is similar.

4.2.1. Short waves $\beta \rightarrow \infty$

In fact, the growth rates for short waves are proportional to $([[N_2]])^2$. This is illustrated in the case of $l_1=0.5$ shown in Fig. 8. Note that between the curves for doubling the $[[N_2]]$ from -0.0435 to -0.087 , the growth rates jump by a factor 4.

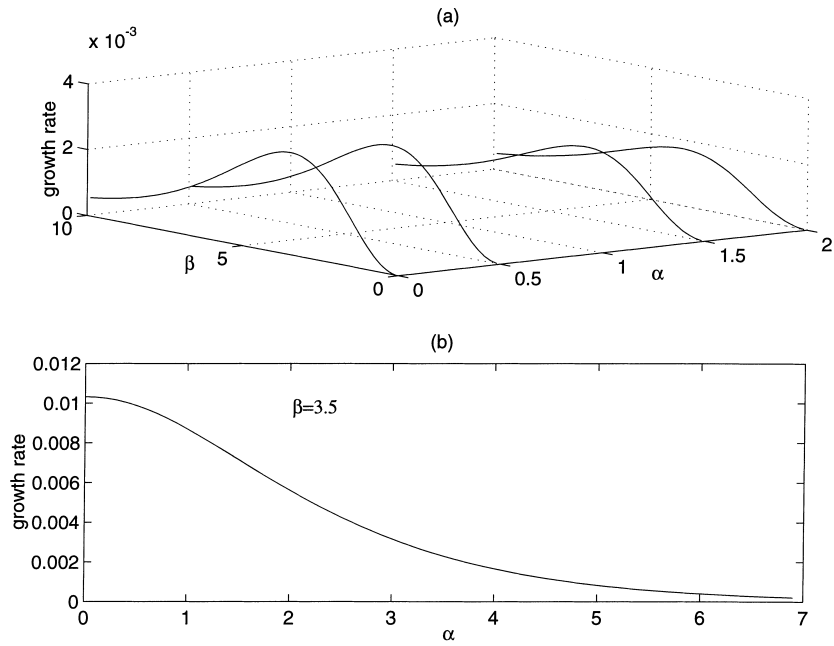


Fig. 5. Growth rates $\text{Re } \sigma$ vs (a) wavenumbers α and β at parameters given in row 1 of Table 1, (b) streamwise wavenumbers α at the spanwise wavenumber of maximum growth rate.

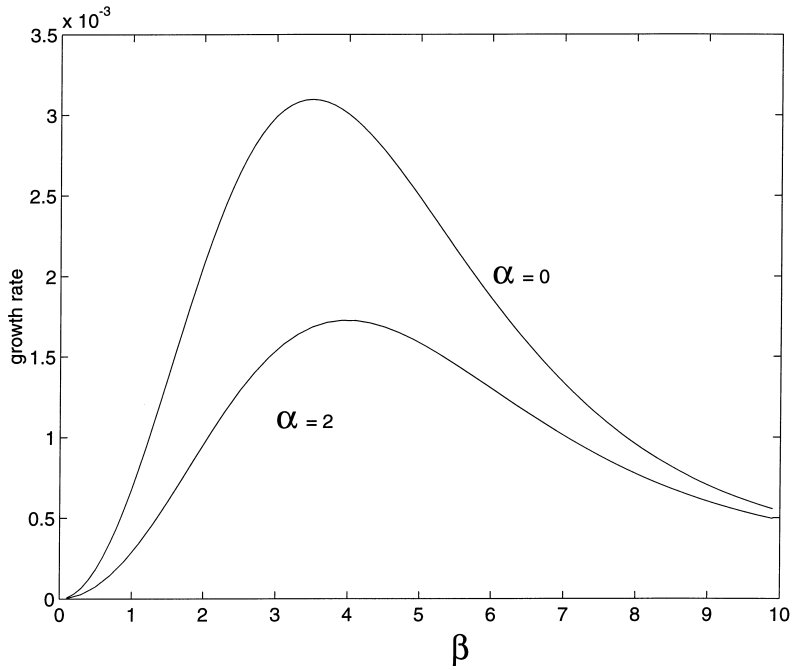


Fig. 6. Growth rates $\text{Re } \sigma$ vs spanwise wavenumbers β at streamwise wavenumbers $\alpha=0,2$, parameters given in row 1 of Table 1.

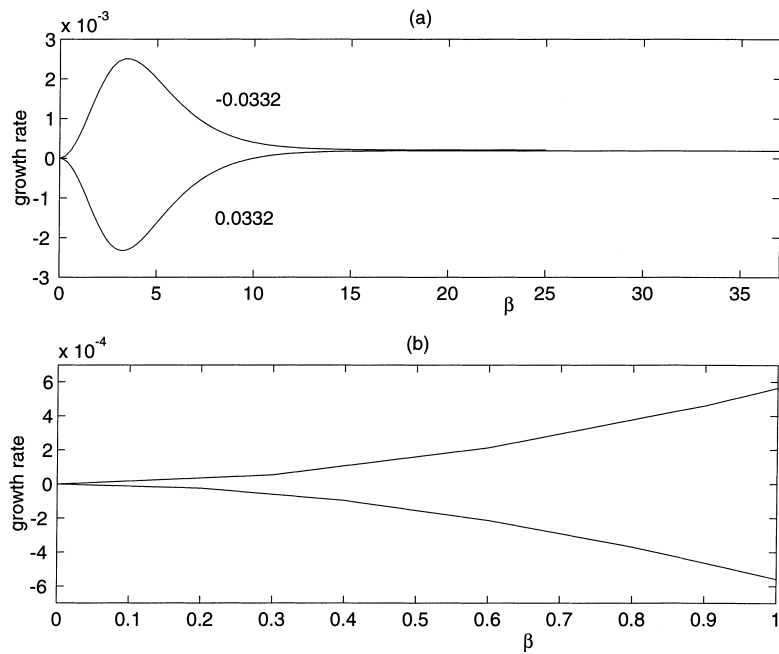


Fig. 7. Growth rates $\text{Re } \sigma$ vs spanwise wavenumbers, β , $\alpha=0$, at parameters given in rows 2 and 3 of Table 1, for which $[[N_2]] = -0.0332$ (upper curve) and 0.0332 (lower), respectively. (a) shows the curves are close in the short-wave limit, and (b) shows that the growth rates for long waves are proportional to the jump in N_2 .

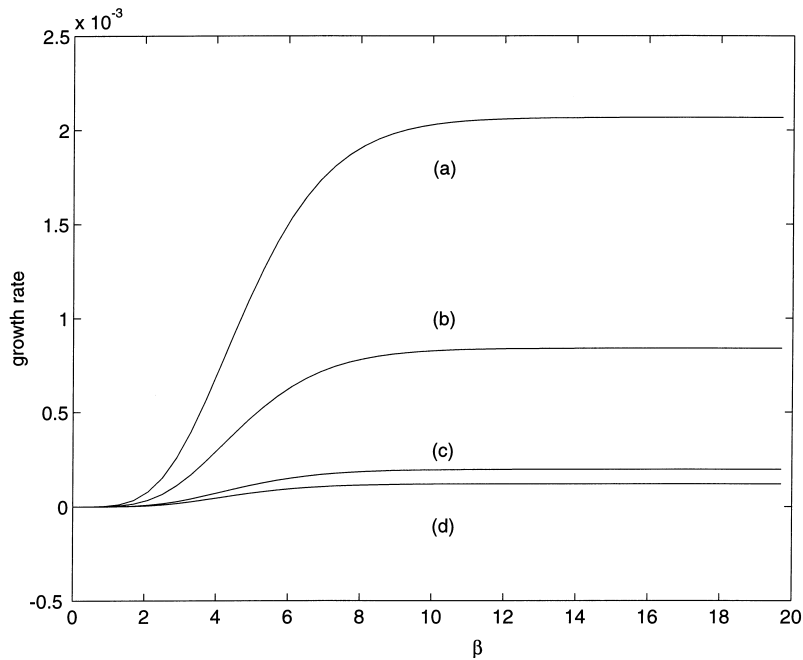


Fig. 8. Growth rates $\text{Re}(\sigma)$ vs spanwise wavenumbers β , at $\alpha=0$, at parameters given in Table 2. The jump in N_2 is (a) -0.132 , (b) -0.087 , (c) -0.0435 , (d) -0.036 .

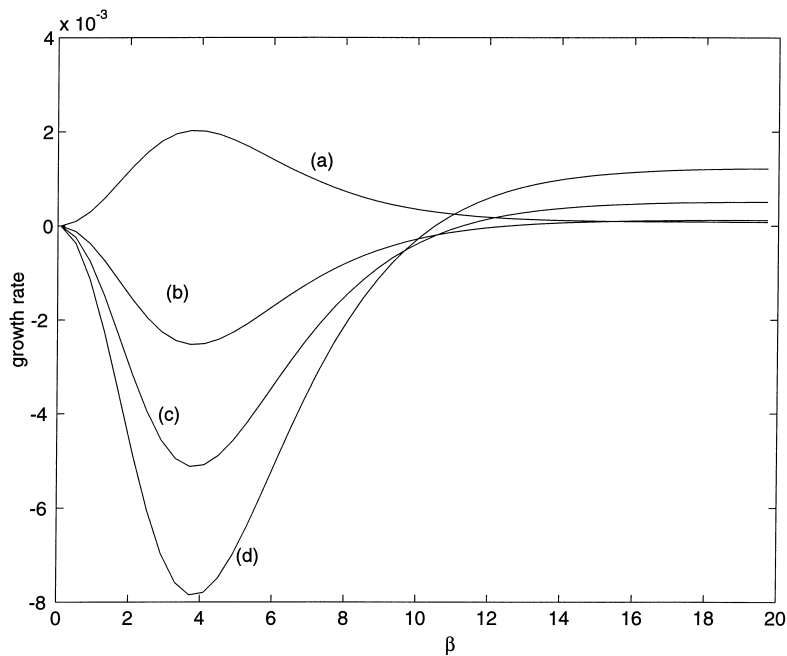


Fig. 9. Growth rates $\text{Re } \sigma$ vs spanwise wavenumbers β , $\alpha=0$, at $l_1=0.7$. The jump in N_2 is (a) 0.0534, (b) -0.0413 , (c) -0.0833 , (d) -0.126 .

4.2.2. Long waves $\beta \rightarrow 0$

For the case of long waves, growth rates are proportional to the jump in N_2 (see Fig. 7). This proportionality persists for order one waves, but eventually the short waves are unstable.

At depth ratio $l_1=0.5$, long waves have zero growth rates, as evident from Fig. 8. In other words, this depth ratio is the one at which $\text{Re } \sigma = f \llbracket N_2 \rrbracket$ and as l_1 varies from 0 to 1, f flips its sign. The growth rates at $l_1=0.7$ are shown in Fig. 9, illustrating this reversal in sign from the case of $l_1=0.3$ shown in Figs. 6 and 7.

4.3. Situations with jumps in both normal stress differences

The combined effect of jumps in both N_1 and N_2 is illustrated in Fig. 10(a) and (b). The parameters are close to the situation of the second row of Table 1. The only change is that the value of W_2 is 1.5 in (a) and $4/3$ in (b). The maximum of each curve is indicated by asterisks. The results for various values of α show that the maximum growth rate mode in (a) is at $\alpha=0$, $\beta=3.6$ which is similar to Fig. 5. However, the introduction of $\llbracket N_1 \rrbracket$ has pushed the $\alpha=3, 4$ modes up so that their maxima are close to that of $\alpha=0$. In this situation, a mix of these modes may be observed. The effect of increasing $\llbracket N_1 \rrbracket$ is that the growth rate for the $\alpha=0$ mode stays the same, but the growth rates for streamwise waves increase, and a finite α mode, e.g. $\alpha=3$ in (b), produces the maximum growth rate mode. The maximum in (b) takes place for a streamwise mode $\beta=0$ rather than oblique or spanwise. Two scenarios for the observation of oblique waves are, first, that experiments such as those of [15] force specific long waves or at most $\alpha=1$ or 2. Higher values of α are ruled out. In this case, the presence of $\llbracket N_1 \rrbracket$ as shown

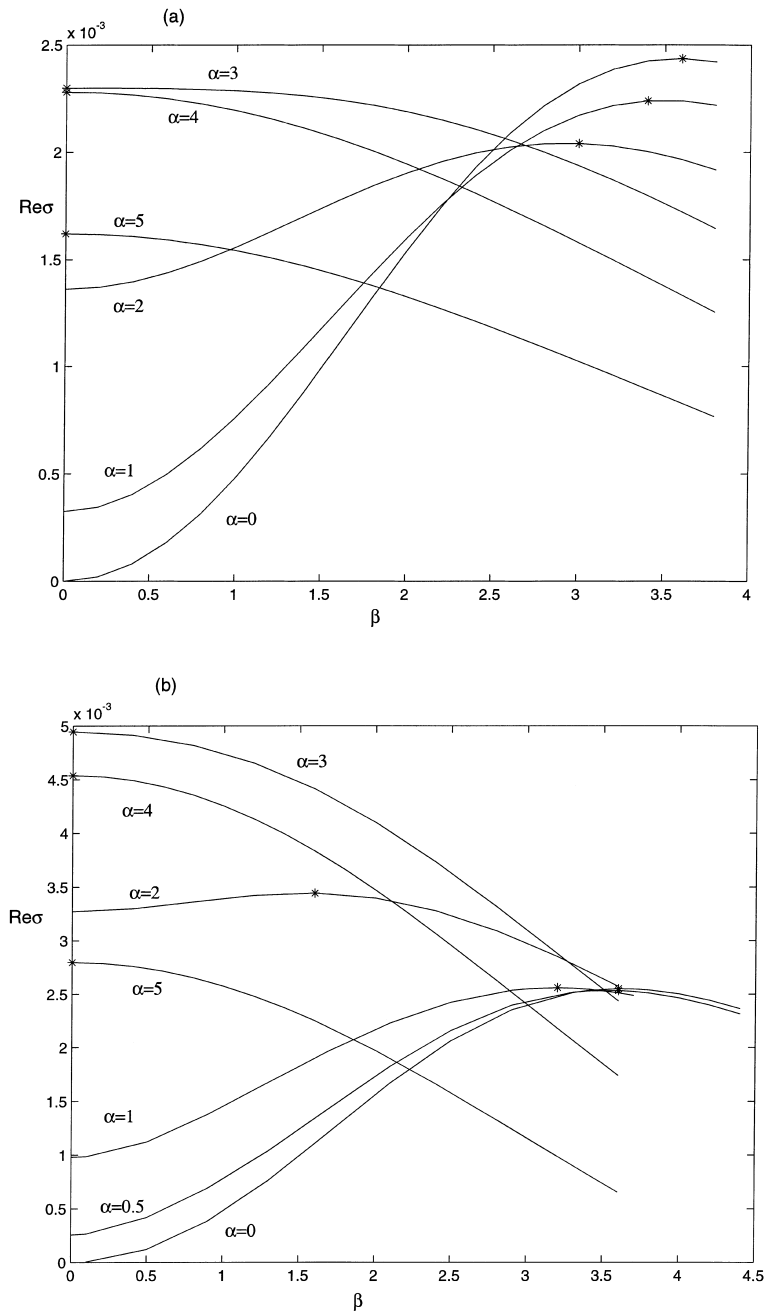


Fig. 10. Growth rates $\text{Re}\sigma$ vs spanwise wave numbers β , at various choices of $\alpha=0$, at $l_1=0.3$, $R_1=0.001$, $\kappa_1=0.4$, $\kappa_2=0.346$, $m=1.08766$, $W_1=5/3$ (a) $W_2=1.5$. $\llbracket N_2 \rrbracket = -0.045$, $\llbracket N_1 \rrbracket = 0.13$. (b) $W_2=4/3$. $\llbracket N_2 \rrbracket = -0.06$, $\llbracket N_1 \rrbracket = 0.28$. Asterisks denote maxima.

in (b) produces an oblique wave as the maximum growth rate mode. Secondly, the introduction of interfacial tension stabilizes higher α modes, while lower wavenumbers are left unstable, and results in a maximum growth rate for an oblique wave with both α and β non-zero.

5. Analytic approximation for $|\sigma W_i| \ll 1$ and $\mathbf{R}=0$

We seek normal mode solutions to the perturbation equations in the appendix which are proportional to $\exp(i\beta y + \sigma t)$ (i.e. there is no x -dependence), and we assume that $|\sigma W_i|$ is small. We can then neglect the term $W_i(\partial \mathbf{T} / \partial t)$ in the constitutive equation. In addition, we assume zero Reynolds number. In that case, the equations in fluid i assume the form

$$\begin{aligned} W_i[-2C_2 u' - 2T_{13} + \kappa(2C_1 T_{11} + 2C_2 T_{13})] + T_{11} &= 0, \\ W_i[-C_2 v' - T_{23} + \kappa(C_1 T_{12} + C_2 T_{23})] + T_{12} - \frac{\mu_i}{\mu_1} i\beta u &= 0 \\ W_i[-C_3 u' - C_2 w' - T_{33} + \kappa[C_2(T_{11} + T_{33}) + T_{13}(C_1 + C_3)]] + T_{13} - \frac{\mu_i}{\mu_1} u' &= 0, \\ T_{22} - 2\frac{\mu_i}{\mu_1} i\beta v &= 0, \\ W_i[-C_3 v' + \kappa(C_3 T_{23} + C_2 T_{12})] + T_{23} - \frac{\mu_i}{\mu_1} (v' + i\beta w) &= 0 \\ W_i[-2C_3 w' + \kappa(2C_2 T_{13} + 2C_3 T_{33})] + T_{33} - 2\frac{\mu_i}{\mu_1} w' &= 0 \\ i\beta v + w' = 0, i\beta T_{12} + T'_{13} = 0, i\beta(T_{22} - p) + T'_{23} = 0, i\beta T_{23} + T'_{33} - p' &= 0. \end{aligned} \quad (15)$$

These equations form an ordinary differential-algebraic system with constant coefficients, which can be solved in closed form. This was done using Mathematica. There are six linearly independent solutions, which are of the form

$$(\mathbf{T}, \mathbf{u}, p) = \mathbf{q}_k \exp(r_k z), \quad k = 1, \dots, 6, \quad (16)$$

where the vector \mathbf{q}_k is independent of z . Since the differential system is of sixth order, one would generally expect the r_k to be determined by a sixth degree polynomial. This polynomial can, however, be factored into quadratic terms, yielding r_k to be one of the following:

$$\begin{aligned} \pm \beta \sqrt{\frac{1}{1 + 2C_3 \kappa_i W_i}}, \quad \pm \sqrt{\frac{2\mu_i/\mu_1(1 + (C_1 + C_3)\kappa_i W_i)}{(\mu_i/\mu_1 + C_3 W_i)(2 + (C_1 + C_3)\kappa_i W_i)}}, \\ \pm \beta \sqrt{\frac{\mu_i/\mu_1(1 + 2C_1 \kappa_i W_i + 2C_3 \kappa_i W_i + 4C_2 \kappa_i W_i^2 - 4C_2^2 \kappa_i^2 W_i^2 + 4C_1 C_3 \kappa_i^2 W_i^2)}{(\mu_i/\mu_1 + C_3 W_i)(1 + (C_1 + C_3)\kappa_i W_i)}}. \end{aligned} \quad (17)$$

We can now represent the solution in each fluid as a linear combination of these six linearly independent solutions:

$$(\mathbf{T}, \mathbf{u}, p) = \sum_{k=1}^6 \gamma_k \mathbf{q}_k \exp(r_k(z - l_1)); \quad (18)$$

this yields twelve undetermined coefficients (six in each fluid). We must satisfy the boundary conditions

$$u = v = w = 0 \tag{19}$$

at $z=0$ and $z=1$, and the interface conditions. For the case of matched shear rates and first normal stresses, the interface conditions are

$$[[u]] = [[v]] = [[w]] = [[T_{13}]] = [[T_{33} - p]] = \sigma [[T_{23}]] + i\beta w [[C_3]] = 0. \tag{20}$$

The boundary and interface conditions yield twelve equations for the twelve coefficients γ_k , and the eigenvalue σ is determined by setting the determinant of the resulting 12×12 matrix equal to zero. Unfortunately, the resulting expressions are too complicated to produce a “formula” for σ . What we can do, however, is to compute the 12×12 -matrix symbolically, and then insert numerical values of the parameters to evaluate the determinant.

We compare results of the analytical and numerical solutions for the following parameters: $W_1=50$, $W_2=31.1299$, $\kappa_1=0.4$, $\kappa_2=0.336508$, $m=3.36508$, $l_1=0.01$. This is, in a sense, a “bad” case, since σW_1 reaches values up to approximately 0.15, much higher than what is typically attained at more moderate Weissenberg numbers. For $q=0.1$, $[[N_2]] = -0.0105$, Fig. 11 shows the growth rate as a function of the wavenumber calculated from a numerical solution of the full equations, while Fig. 12 shows the growth rate calculated from the analytical procedure used above. The maximum difference is approximately 10%. We note that numerical computations for large β require a large number of Chebyshev modes ($\gg \beta$) and therefore longer CPU time. In contrast, the time to compute the analytic solution is

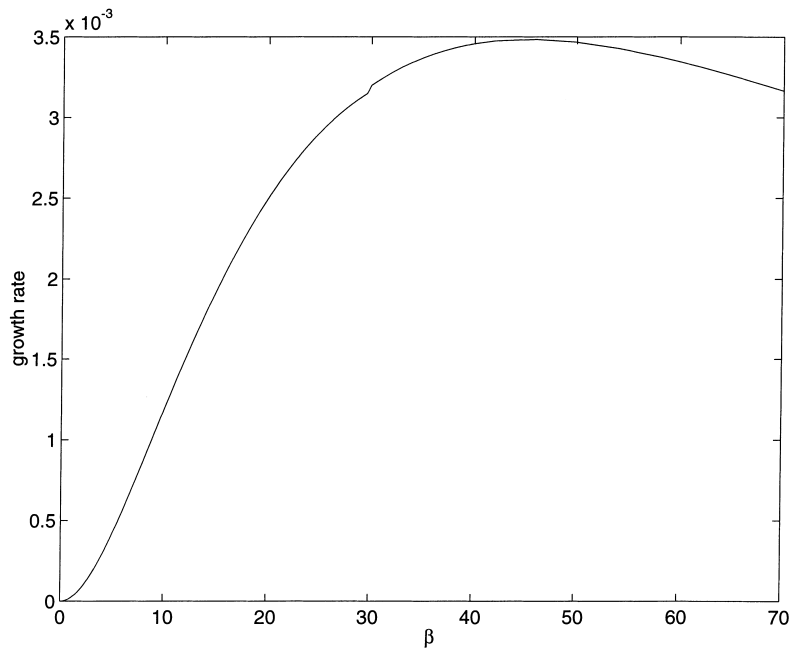


Fig. 11. Numerical solution for growth rate $\text{Re } \sigma$ vs β at $\alpha=0$, $W_1=50$, $W_2=31.13$, $\kappa_1=0.4$, $\kappa_2=0.337$, $m=3.365$, $l_1=0.01$.

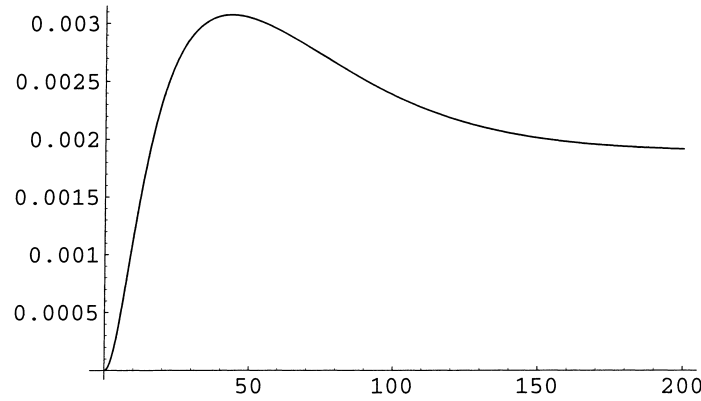


Fig. 12. Analytical solution for growth rate $\text{Re } \sigma$ vs β at $\alpha=0$, $W_1=50$, $W_2=31.13$, $\kappa_1=0.4$, $\kappa_2=0.337$, $m=3.365$, $l_1=0.01$.

independent of β (it took approximately 3 s per data point on a Mac PowerBook 520). The results show the growth rate going through a maximum when β is approximately 43.5; this is a fairly long wave relative to the thickness of the layer occupied by fluid 1; as β approaches infinity, the growth rate tends to a limit which is essentially of the same order as the maximum growth rate. This suggests that interface distortions resulting from these instabilities would be irregular rather than periodic.

6. Analysis of the spectrum for $\mathbf{R}=0$

If we do not assume that $|\sigma W_i|$ is small, we can start our analysis in principle in the same fashion as in Section 5. We now retain the term $\sigma W_i T$ in the constitutive equation. We still obtain a differential-algebraic system with constant coefficients in each fluid; the coefficients, however, depend on σ now. Instead of Eq. (17), we find the roots r_k to be (the derivation was done using Mathematica)

$$\begin{aligned} & \pm \beta \sqrt{\frac{1 + \sigma W_i}{1 + 2C_3 \kappa_i W_i + \sigma W_i}}, \\ & \pm \beta \sqrt{\frac{2(\mu_i/\mu_1)(1 + (C_1 + C_3)\kappa_i W_i + \sigma W_i)}{(\mu_i/\mu_1 + C_3 W_i)(2 + (C_1 + C_3)\kappa_i W_i + 2\sigma W_i)}}, \\ & \pm \beta \sqrt{\frac{(\mu_i/\mu_1)((1 + 2(C_1 + C_3)\kappa_i W_i + \sigma W_i)(1 + \sigma W_i) + 4\kappa_i W_i^2(C_2 - C_2^2 \kappa_i + C_1 C_3 \kappa_i))}{(1 + \sigma W_i)(\mu_i/\mu_1 + C_3 W_i)(1 + (C_1 + C_3)\kappa_i W_i + \sigma W_i)}}. \end{aligned} \quad (21)$$

These roots are determined by the differential equations. In principle, we can now proceed as in Section 5, and obtain the eigenvalues σ by setting a 12×12 -determinant equal to zero. This leads to a transcendental equation, due to the appearance of the expressions $\exp(-r_k l_1)$ and $\exp(r_k l_2)$ in the boundary conditions.

6.1. Short waves

A simplification arises if we consider the limit of short spanwise waves $\beta \rightarrow \infty$. In this case, we can limit our attention to perturbations which decay exponentially away from the interface, and we ignore the effect of the boundaries. That is, in Eq. (18), we include only those r_k which have positive real part in fluid 1, and only those with negative real part in fluid 2. This leads to three undetermined coefficients in each fluid, and the interface conditions determine σ as the root of a 6×6 -determinant. This determinant now involves only expressions which are polynomials in σ or square roots of polynomials in σ , and, in principle, we can reduce everything to a polynomial in σ by repeated squaring. Unfortunately, the expressions are too complicated to actually carry this out. The problem is similar to the case of streamwise perturbations in two-layer Couette flow of upper convected Maxwell fluids [9], where the short wave limit of the interfacial eigenvalue leads to a fifth degree polynomial. In the present situation, the degree of the polynomial to be analyzed would be quite large, certainly in the hundreds. We therefore present below the mathematically related but tractable analysis of wall modes.

7. The spectrum for single-fluid flow, $R=0$

7.1. Non-existence of spanwise wall modes

We shall focus on a simpler, but mathematically similar problem. For this, we consider modes which are confined close to one of the walls, and decay exponentially away from it, such modes are the spanwise analogue of the streamwise Gorodtsov–Leonov modes [3] in the case of the upper convected Maxwell fluid.

We examine short waves close to a wall. The rescaling of the spatial variables to a region close to one of the walls is equivalent to keeping the variables as they are, placing a wall at $z=0$ and taking the fluid domain to be infinite; we take the half-plane $z < 0$.

We are interested in solutions which decay away from the wall, so we look for solutions of the form

$$(\mathbf{T}, \mathbf{u}, p) = \sum_{k=1}^3 \gamma_k \mathbf{q}_k \exp(r_k z), \tag{22}$$

where the sum includes only those r_k from Eq. (21) which have positive real part. Since each r_k contains the factor β , and the perturbation solutions are proportional to $\exp(i\beta y + r_k z)$, we can redefine βy and βz to be the new y and z ; i.e. set $\beta=1$.

The three boundary conditions $u=v=w=0$ at $z=0$ lead to three equations for the coefficients γ_k . We set the resulting determinant equal to zero. Using symbolic manipulation, we were able to show that the resulting equation can be reduced to a sixteenth degree polynomial for σ :

$$\sum_{i=0}^{16} p_i \sigma^i = 0. \tag{23}$$

Interested readers may obtain a copy of the Mathematica file and of the expressions for the p_i on request. We chose not to include the results, since they would take up approximately six printed pages.

We shall supply these formulae to interested readers on request; the problem is far from trivial and pushes the limits of Mathematica's capabilities. The printout of the expressions for the coefficients p_i is approximately six pages long.

We can, however, not claim that the sixteen roots of the polynomial lead to eigenvalues. This is because the expressions for the r_k from Eq. (21) involve square roots, and the polynomial was obtained by repeated squaring. We need to go back to the original equations and check whether the square roots are "on the right branch." That is, the r_k need to have positive real parts in order to actually yield wall modes; if r_k has a negative real part, then we would instead have a solution growing exponentially away from the wall which has no physical meaning.

To illustrate what happens, consider the simple equation

$$\sqrt{f} + 2 = 0 \quad (24)$$

to be solved for f . The domain of this complex-valued square root function consists of two Riemann sheets, one which yields the square root with positive real part (e.g. $\sqrt{4} = 2$), and the other yielding the root with negative real part (e.g. $\sqrt{4} = -2$). Note that for the wall modes which decay like $\exp(-r_k z)$, we seek those r_k which have a positive real part. Translated to the analogy of Eq. (24), the \sqrt{f} denotes the branch with positive real part. It is then obvious that there is no solution. On the other hand, if we blindly write $\sqrt{f} = -2$ and square the equation, we obtain $f=4$, which actually satisfies the equation $-\sqrt{f} + 2 = 0$ rather than Eq. (24). A similar check needs to be done for the sixteen roots of the polynomial found above. We did so and found that all of them are on the branch with the undesired sign for the real part, i.e. none of them actually yield any eigenvalues. This shows that there are no wall modes for spanwise perturbations to the flow.

7.2. Continuous spectra and stress relaxation modes

The analysis of continuous spectra for single-fluid flows immediately applies also to two-fluid flows. The zeros of the denominators of the expressions in Eq. (21) yield continuous spectra and the zeros of the numerators yield stress relaxation modes as shown below.

If the denominator of one of the r_k is zero, then the differential system governing the linear stability problem is singular. These singular values of σ show up in the numerical computations of the spectrum as accumulation points, and are continuous spectra of the original problem.

Stress relaxation modes are defined as eigenfunctions which have zero velocities and stresses independent of z (cf Eq. (18)). For such perturbations, the equations in the appendix yield $T_{12}=T_{23}=0$, $p=T_{22}$, and, in addition,

$$\begin{aligned} T_{11} + W_i[\sigma T_{11} - 2T_{13} + \kappa_i(2C_1 T_{11} + 2C_2 T_{13})] &= 0, \\ T_{13} + W_i[\sigma T_{13} - T_{33} + \kappa_i((C_1 + C_3)T_{13} + C_2(T_{11} + T_{33}))] &= 0, \\ T_{33} + W_i[\sigma T_{33} + \kappa_i(2C_2 T_{13} + 2C_3 T_{33})] &= 0, \\ T_{22}(1 + \sigma W_i) &= 0. \end{aligned} \quad (25)$$

The eigenvalues of this system are precisely the zeros of the numerators of the r_k . We compare this analysis of the roots of the numerators with a full numerical computation of the single-fluid case $q=0.4$ of Table 2, $l_1=0.5$, $R_1=0.001$, $\kappa_1=\kappa_2=0.4$, $W_1=W_2=1$, $C_1=0.843$, $C_2=0.648$, $C_3=-0.181$. In this case,

Table 2

Fluid 1 parameters are $l_1=0.5$, $R_1=0.001$, $\kappa_1=0.4$, $W_1=1$, $C_1=0.843$, $C_2=0.648$, $C_3=-0.181$. Fluid 2 parameters are tabulated

W_2	$[[N_2]]$	q	m	κ_2
0.875	-0.132	0.1	1.317	0.132
0.935	-0.087	0.2	1.171	0.234
0.976	-0.044	0.3	1.070	0.321
1.007	0.036	0.48	0.959	0.460

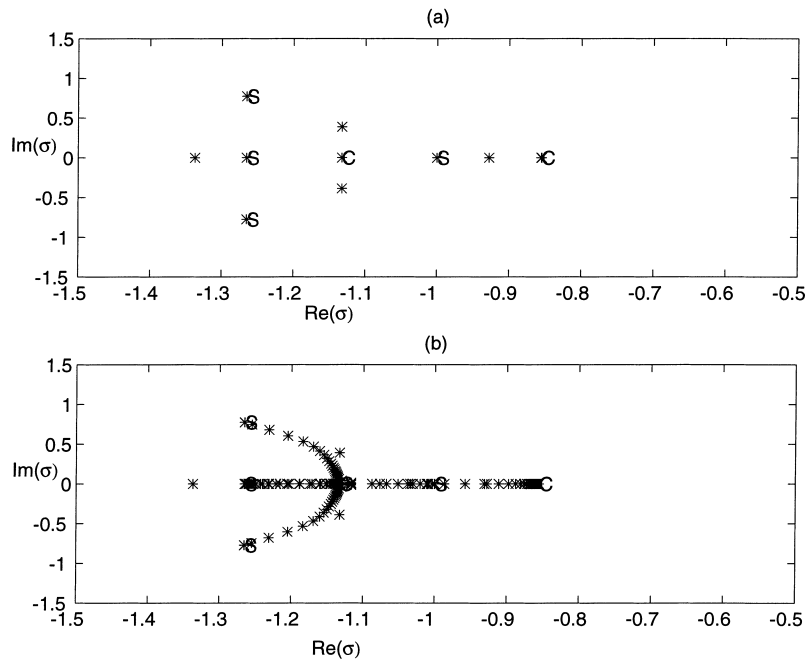


Fig. 13. Numerical solution for growth rate $\text{Re } \sigma$ vs $\text{Im } \sigma$ at (a) $\beta=0$, (b) $\beta=10$, $l_1=0.5$, $R_1=0.001$, $\kappa_1=\kappa_2=0.4$, $W_1=W_2=1$.

the eigenvalues for the stress relaxation modes (i.e. the values of σ which make the numerators of the r_k equal to zero) are -1 , -1.2648 and $-1.2648 \pm 0.7748i$; the values of the singular modes that are limits of the continuous spectra for the problem with streamwise disturbances are -1 , -1.2648 , -0.8552 and -1.1324 . Fig. 13 shows the numerical results at (a) $\beta=0$ and (b) $\beta=10$. The number of eigenvalues in the picture increases with β . The modes listed above are denoted by S for stress relaxation modes and C for the latter two of the continuous spectra. These modes remain the same irrespective of β , as evident from the full numerical calculation.

Acknowledgements

This research was sponsored by the National Science Foundation under Grants No. CTS-9612308 and DMS-9622735.

Appendix. Perturbation equations for parallel flow

In the base flow, the stresses C_i are constants in each fluid. The constitutive equations are

$$W_i \left[\frac{\partial T_{11}}{\partial t} + U \frac{\partial T_{11}}{\partial x} - 2 \frac{\partial u}{\partial x} C_1 - 2 \frac{\partial u}{\partial z} C_2 - 2U'T_{13} + \kappa_i(2C_1T_{11} + 2C_2T_{13}) \right] + T_{11} - \frac{2\mu_i}{\mu_1} \frac{\partial u}{\partial x} = 0, \quad (\text{A1})$$

$$W_i \left[\frac{\partial T_{12}}{\partial t} + U \frac{\partial T_{12}}{\partial x} - \frac{\partial v}{\partial x} C_1 - \frac{\partial v}{\partial z} C_2 - U'T_{23} + \kappa_i[T_{12}C_1 + C_2T_{23}] \right] + T_{12} - \frac{\mu_i}{\mu_1} \left(\frac{\partial u}{\partial y} + \frac{\partial v}{\partial x} \right) = 0, \quad (\text{A2})$$

$$W_i \left[\frac{\partial T_{13}}{\partial t} + U \frac{\partial T_{13}}{\partial x} - \frac{\partial u}{\partial z} C_3 - \frac{\partial w}{\partial z} C_2 - \frac{\partial u}{\partial x} C_2 - \frac{\partial w}{\partial x} C_1 - U'T_{33} + \kappa_i[C_2(T_{11} + T_{33}) + T_{13}(C_1 + C_3)] \right] + T_{13} - \frac{\mu_i}{\mu_1} \left(\frac{\partial u}{\partial z} + \frac{\partial w}{\partial x} \right) = 0, \quad (\text{A3})$$

$$W_i \left[\frac{\partial T_{22}}{\partial t} + U \frac{\partial T_{22}}{\partial x} \right] + T_{22} - \frac{2\mu_i}{\mu_1} \frac{\partial v}{\partial y} = 0, \quad (\text{A4})$$

$$W_i \left[\frac{\partial T_{23}}{\partial t} + U \frac{\partial T_{23}}{\partial x} - \frac{\partial v}{\partial z} C_3 - \frac{\partial v}{\partial x} C_2 + \kappa_i(T_{23}C_3 + T_{12}C_2) \right] + T_{23} - \frac{\mu_i}{\mu_1} \left(\frac{\partial v}{\partial z} + \frac{\partial w}{\partial y} \right) = 0, \quad (\text{A5})$$

$$W_i \left[\frac{\partial T_{33}}{\partial t} + U \frac{\partial T_{33}}{\partial x} - 2 \frac{\partial w}{\partial x} C_2 - 2 \frac{\partial w}{\partial z} C_3 + \kappa_i(2T_{13}C_2 + 2T_{33}C_3) \right] + T_{33} - \frac{2\mu_i}{\mu_1} \frac{\partial w}{\partial z} = 0. \quad (\text{A6})$$

Continuity is

$$\frac{\partial u}{\partial x} + \frac{\partial v}{\partial y} + \frac{\partial w}{\partial z} = 0. \quad (\text{A7})$$

The equations of motion in each fluid yield

$$R \left[\frac{\partial u}{\partial t} + U \frac{\partial u}{\partial x} + wU' \right] + \frac{\partial p}{\partial x} - \left(\frac{\partial T_{11}}{\partial x} + \frac{\partial T_{12}}{\partial y} + \frac{\partial T_{13}}{\partial z} \right) = 0, \quad (\text{A8})$$

$$R \left[\frac{\partial v}{\partial t} + U \frac{\partial v}{\partial x} \right] + \frac{\partial p}{\partial y} - \left(\frac{\partial T_{12}}{\partial x} + \frac{\partial T_{22}}{y} + \frac{\partial T_{23}}{\partial z} \right) = 0, \quad (\text{A9})$$

$$R \left[\frac{\partial w}{\partial t} + U \frac{\partial w}{\partial x} \right] + \frac{\partial p}{\partial z} - \left(\frac{\partial T_{13}}{\partial x} + \frac{\partial T_{23}}{\partial y} + \frac{\partial T_{33}}{\partial z} \right) = 0. \quad (\text{A10})$$

The boundary conditions are $u=v=w=0$ at $z=0,1$. The conditions at the interface are posed at $z=l_1+h(x,y,t)$. The unknown $h(x,y,t)$ is assumed to be small; the interfacial conditions are expanded as Taylor series about $z=l_1$, and terms up to cubic order are retained [11,13].

Continuity of velocity yields

$$h[[U']] + [[u]] = 0, \quad [[v]] = 0, \quad [[w]] = 0, \quad (\text{A11})$$

where $[[x]]$ denotes $x(\text{fluid 1}) - x(\text{fluid 2})$. Continuity of shear stress yields

$$[[T_{13}]] + \frac{\partial h}{\partial x} [[C_3 - C_1]] = 0, \quad (\text{A12})$$

where $[[C_2]] = 0$ from the base flow shear stress balance and $C'_2 = 0$ from the base flow x-momentum equation, and

$$[[T_{23}]] + [[C_3]]h_y = 0. \quad (\text{A13})$$

The balance of normal stress yields

$$[[T_{33}]] - [[p]] = 0. \quad (\text{A14})$$

The kinematic free surface condition yields

$$\frac{\partial h}{\partial t} + U(l_1) \frac{\partial h}{\partial x} - w_1 = 0. \quad (\text{A15})$$

References

- [1] K. Chen, Elastic instability of the interface in Couette flow of viscoelastic fluids, *J. Non-Newtonian Fluid Mech.* 40 (1991) 261.
- [2] K. Chen, Interfacial instabilities in stratified shear flows involving multiple viscous and viscoelastic fluids, *Appl. Mech. Rev.* 48 (1995) 763.
- [3] V.A. Gorodtsov, A.I. Leonov, On a linear instability of a plane parallel Couette flow of a viscoelastic fluid, *J. Appl. Math. Mech. (PMM)* 31 (1967) 310.
- [4] T. Hagen, M. Renardy, Boundary layer analysis of the Phan-Thien–Tanner and Giesekus models in high Weissenberg number flow, *J. Non-Newtonian Fluid Mech.* 73 (1997) 181.
- [5] E.J. Hinch, O.J. Harris, J.M. Rallison, The instability mechanism for two elastic liquids being co-extruded, *J. Non-Newtonian Fluid Mech.* 43 (1992) 311.
- [6] D.D. Joseph, Y.Y. Renardy, *Fundamentals of Two-Fluid Dynamics, Part I: Mathematical Theory and Applications; Part II: Lubricated Pipelining, Drops and Miscible Liquids*, Springer Verlag New York, 1993.
- [7] R.G. Larson, Instabilities in viscoelastic flows, *Rheol. Acta* 31 (1992) 213.
- [8] S.A. Orszag, Accurate solutions of the Orr–Sommerfeld stability equation, *J. Fluid Mech.* 50 (1971) 689.
- [9] Y. Renardy, Stability of the interface in two-layer Couette flow of upper convected Maxwell liquids, *J. Non-Newtonian Fluid Mech.* 28 (1988) 99.
- [10] Y. Renardy, Spurt and instability in a two-layer Johnson–Segalman liquid, *Theor. Comp. Fluid Dyn.* 7 (1995) 463.
- [11] Y. Renardy, Weakly nonlinear behavior of periodic disturbances in two-layer plane channel flow of upper-convected Maxwell liquids, *J. Non-Newt. Fluid Mech.* 56 (1995) 101.

- [12] Y. Renardy, An instability of plane Couette flow of the Johnson-Segalman liquid, in *Advances in Multi-Fluid Flows*, eds. Y. Renardy, A.V. Coward, D.T. Papageorgiou, S.M. Sun, SIAM (1996), 199.
- [13] Y. Renardy, B. Khomami, K.C. Su, M.A. Clarke, An experimental/theoretical investigation of interfacial stability in superposed pressure-driven channel flow of viscoelastic fluids, in preparation (1997).
- [14] Y.Y. Su, B. Khomami, Purely elastic interfacial instabilities in superposed flow of polymeric fluids, *Rheol. Acta* 31 (1992) 413.
- [15] G.M. Wilson, B. Khomami, An experimental investigation of interfacial instabilities in multilayer flow of viscoelastic fluids. II. Elastic and nonlinear effects in incompatible polymer systems, *J. Rheol.* 37 (1993) 315.